Turkish Journal of Electrical Engineering & Computer Sciences

http://journals.tubitak.gov.tr/elektrik/

Research Article

Turk J Elec Eng & Comp Sci
(2020) 28: 1916 – 1931

doi:10.3906/elk-1909-115

Harmonic reduction of SVC with system integrated APF

Xuhui YAN[1], **Feng WANG**[1], **Mahmood UL HASSAN**[2], **Muhammad HUMAYUN**[3,*]
[1]State Grid Liyang Power Supply Company, Liyang, Jiangsu, China
[2]Institute of Plasma Physics, Chinese Academy of Sciences, Hefei, China
[3]School of Electronics Information and Electrical Engineering,
Shanghai Jiao Tong University, Shanghai, P.R. China

Received: 21.09.2019 • **Accepted/Published Online:** 20.01.2020 • **Final Version:** 29.07.2020

Abstract: Static VAR compensators (SVCs) are widely used to compensate for reactive power in a system. The hybrid active power filter (HAPF) in combination with SVC has extensively been studied in the literature to reduce harmonics generated by the SVC. This study proposes a new topology of SVC for three-phase systems based on a three-phase thyristor-control reactor (TCR). The harmonics generated by the TCR are minimized by an active power filter (APF), which can be realized by a reduced resonant capacitor size. A control strategy comprising feedback and feedforward control is employed to achieve good harmonic reduction and fast transient response. Simulated and experimental results are presented to validate the theoretical analysis and performance of the proposed topology and control scheme. The results show that the proposed topology can mitigate the harmonics generated by the TCR.

Key words: Static VAR compensators (SVC), active power filters (APF), feedback control, feedforward control, DC-link control

1. Introduction

In recent years, the development and use of electronic devices to improve stability and efficiency of power systems has seen a significant increase in the industry. However, the power quality standards have to be strictly followed when using these devices. It has also been found that such devices introduce harmonic currents into the grid [1–5]. Since the proliferation of nonlinear loads has resulted in a significant increase in reactive power, voltage fluctuations, line losses, and phase imbalances, recent research has mostly focused on the electrical power quality of the power systems [6, 7].

Static compensator (STATCOM) has been extensively studied in the technical literature. Good, efficient, and robust design makes the SVC a better choice for load balancing and reactive power compensation [8]. Active power filters (APFs) have been widely used to improve the power quality and to mitigate harmonics that increase system efficiency [9–11]. The control algorithms for APF have been studied in depth, and researchers continue to improve this control technique [12, 13]. $I_{L_A}\, I_{C_A}\, I_{TCR_A}$ [A].

An SVC usually consists of a thyristor-controlled reactor (TCR) and fixed capacitors (FCs). When the TCR is operated under unbalanced operating conditions, it generates a significant amount of low-order odd harmonics, which are not difficult to eliminate. In a three-phase application, fifth and seventh harmonics are dominant. Hence, FCs are usually tuned with appropriately sized reactors to act as passive filters (PFs) at

*Correspondence: mhumayun88@sjtu.edu.cn

the characteristic harmonic frequencies generated by the TCR. However, it can produce a series of parallel resonance, which leads to system instability. Recently, several articles have presented combined systems for reactive power compensation and harmonic suppression using SVC and APF [14, 15]. These methods have shown considerable improvement of power quality in microgrid [16] and high-power applications [17]. However, this new combination requires comprehensive control strategies to reduce response time and improve the meticulous design of reference current signal generation techniques.

In order to overcome the aforementioned issues, a new topological structure was proposed [18] by combining a low power voltage source inverter (VSI), which works as an APF, to eliminate the TCR harmonics. Additionally, it can improve the PF and mitigate the conduction and switching losses in the VSI. This hybrid SVC is a combination of an APF, TCR, and PFs. The proposed topology can also reduce the APF control bandwidth requirements with redesigned PF filters and, therefore, make the compensation more economical and accurate. It has been verified that this new topology performs well in a single-phase system [18].

In this work, the topology presented earlier [18] is extended to a three-phase, three-wire system to analyze its performance in a more complex scenario. The application of this topology to the extended system has been made possible by use of a new control algorithm which consists of two parts: a feedback component, to ensure the system stability; and a feedforward component, to increase the system's dynamic response speed.

The rest of the paper consists of the following parts. Section 2 describes the proposed three-phase SVC system, which is followed by the control scheme for the proposed system in Section 3. Simulated and experimental results are presented in Section 4, where the SVC system design and control technique are analyzed, and finally, Section 5 presents a brief conclusion of the work.

2. System description

In this section, the proposed three-phase system is described. For convenience, the single-phase system has been considered first. A static VAR compensator (SVC) consists of bidirectional thyristor, reactors, and capacitors. Several SVC architectures are presented in literature, but two types got more attention. The first one is fixed capacitor (FC) thyristor controlled rectifier (TCR) and the second is thyristor switched capacitors (TSC) TCR. In FC-TCR SVC configuration, a TCR and capacitor are connected in shunt with each other that provides controllable reactive power only in the lagging power factor range. The reactive power (capacitive var) obtained by firing angle (α) of TCR is zero. The capacitive reactive power is decreased by increasing the TCR firing angle [19]. The current in the reactor can be calculated from the following equations:

$$u_{\mathrm{AC}}(t) = U_{\mathrm{DC}} \cos(\omega t), \tag{1}$$

$$i_L = \frac{1}{L}\int_{\alpha}^{\omega t} u_{\mathrm{AC}}(t)dt = \frac{U_m}{\omega L}(\sin(\omega t) - \sin\alpha). \tag{2}$$

Figure 1 shows the simplified evolution of the proposed harmonic-free module with two branches: a single-phase TCR branch and a harmonic filter branch. Conventional design of SVC module is shown in Figure 1a. This PF-based SVC module has a simple structure with a simple controller. However, it requires large values of inductor L and capacitor C for good stability, but lower-order harmonics still exist [20]. Figure 1b shows the SVC module with a series resistor to reduce the values of L and C. This change can significantly decrease the value of inductor and shrink the volume of the SVC module. However, this configuration cannot eliminate low-order harmonics and, with the use of a resistor, the losses of the system will increase; this makes

this approach impractical. Figure 1c shows the proposed design, where the resistor has been replaced by a voltage source inverter (VSI) to increase the system stability and make it more practical. Here L_fC_f is an optional branch that provides a low impedance path to the current. This results in a reduced power rating of the inverter. However, an external DC source is required to maintain VSI DC-link voltages.

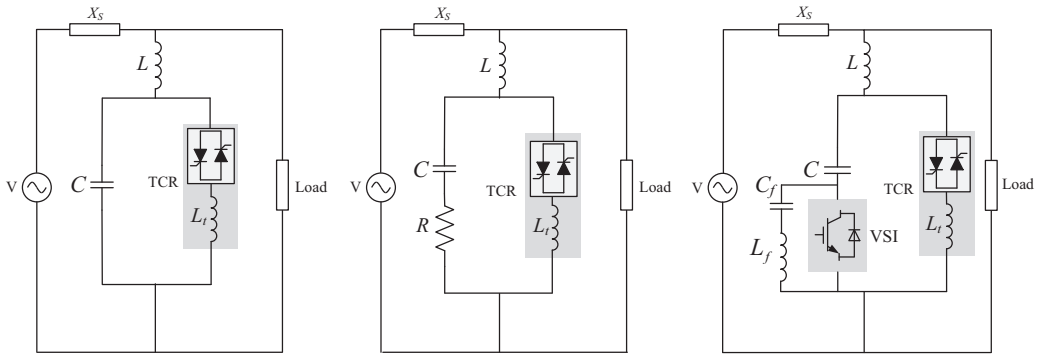

(a) Passive Filter TCR (b) Reduced L TCR module (c) Proposed harmonic-free TCR module

Figure 1. The systematic construction of the proposed SVC module from conventional SVC.

Figure 2 shows the simplified view of the proposed three-phase, three-wire system. In a three-phase system, the power rating of the VSI is $\sqrt{3}$ smaller than the single phase system, so L_fC_f branch has been neglected, while the power for maintaining the DC-link voltage is absorbed through an AC-link of the VSI. The switching harmonic filter branch consists only of inductor $L_i(i \in \{A, B, C\})$, and a VSI is connected in series to C_i directly. In this system, the capacitor C serves two purposes. (1) It provides a means to reduce the voltage rating of the VSI. As all the fundamental frequency voltages appear across the capacitor, this results in a lower cost and lower power rating of the VSI. (2) It produces leading current to compensate lagging load currents. The thyristor control reactor in the TCR block is used to absorb reactive power, whereas the VSI is used to filter out low-order harmonics generated by the TCR and to mitigate the resonant poles of the PFs.

In practical design, the impedance of VSI is almost negligible. Hence, L in combination with C forms a low pass filter on the AC-link side (see bode plot in Figure 7). Based on this fact, the VSI is only tuned to compensate low-order harmonics. The combination of TCR and APF requires a comprehensive controller that would implement the control for the TCR firing angle, for the harmonic compensation, and for the DC-link to maintain the DC-link voltage to a stable level during transient and steady-state conditions.

3. Control strategy

The control strategy of the hybrid system with APF, shown in Figure 3, consists of three groups: (1) The TCR firing angle control, (2) the harmonics compensation control loop for the APF and (3) the DC-link voltage controller. The control loop is a key element of the APF. It further consists of two parts: the feedback control loop and the feedforward component. Different parts of the control strategy and the two components of the controller will be discussed in the following subsections.

3.1. TCR firing angle

Firing angle α control of the thyristor switches regulates the average value of the inductance. The continuously regulated inductance can be used for line flow regulation. TCR is usually used to regulate reactive power of

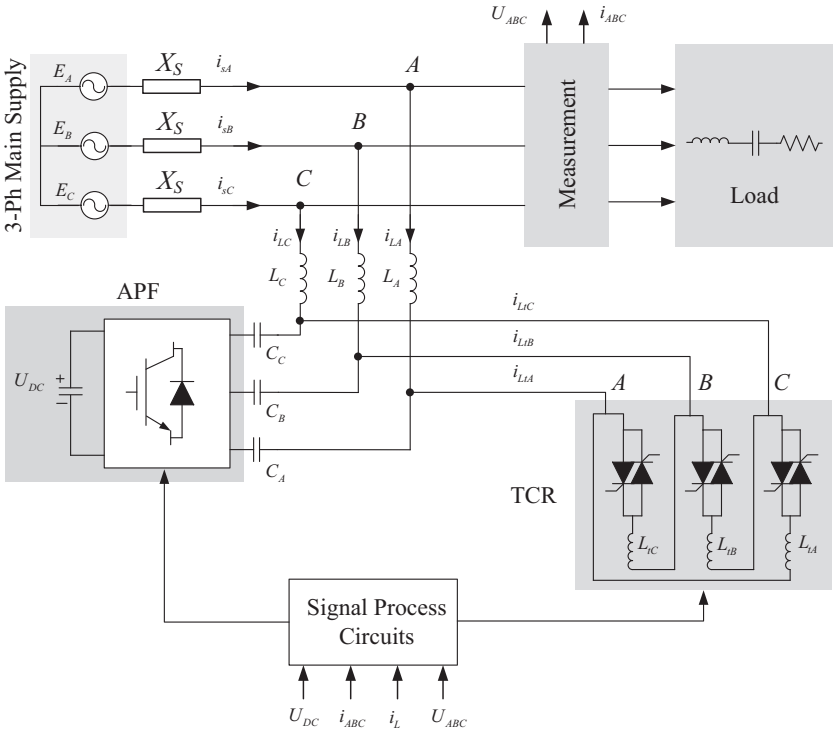

Figure 2. Circuit diagram of the proposed three-phase three-wire hybrid TCR (SVC) system connected to grid and load.

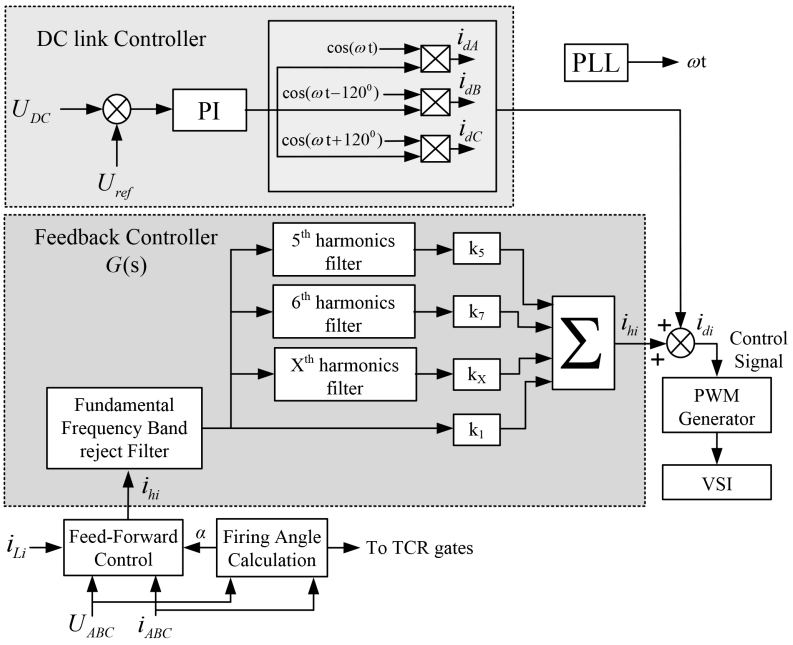

Figure 3. Block diagram of multi-closed loop proposed control scheme for the proposed svc.

the load at point of common coupling in the system [21]. The control of the TCR is based on the control of compensation admittance. In the first step, the fundamental frequency voltage and current of load side are

measured. These values are used to measure the fundamental frequency reactive power. The next step is to estimate required susceptance of SVC to produce required reactive power. As shown in Figure 2 the fundamental frequency model of the system can be obtained by omitting the harmonic components generated by TCR and excluding the harmonic voltages generated by APF. Since APF contribution at fundamental voltages is negligible as compared to line voltages and also it mostly generates voltages at harmonic frequencies, looking from the line side system can be approximated by admittance given by the following equation:

$$B_{SVC} = \frac{B_L(B_{TCR} + B_C)}{B_L + B_{TCR} + B_C}, \tag{3}$$

where $B_C = \omega C$ and $B_L = 1/\omega L$ are the admittance of inductor and capacitor, respectively. B_{SVC} is the required admitance of each SVC module. B_{SVC} can be calculated as:

$$B_{SVC} = \frac{I_{i(rec)}}{U_{AB}} \tag{4}$$

substituting B_{SVC} in Eq. (3) and solving for B_{TCR} we get:

$$B_{TCR} = \frac{B_C \cdot B_L - B_{SVC}(B_C + B_L)}{B_L - B_{SVC}}, \tag{5}$$

The corresponding susceptance of the TCR is given as:

$$B_{TCR} = \frac{1}{3}\frac{g(\alpha)}{\omega L_t}, \tag{6}$$

where $g(\alpha)$ is the firing angle-dependent function and in the literature known as normalized impedance of the TCR inductor. After solving for g(alpha), the firing angle (α) can be obtained from the relation

$$g(\alpha) = 2(\pi - \alpha) + \frac{\sin(2\alpha)}{\pi}. \tag{7}$$

The firing angle α of each phase can be estimated through Eqs. (5)–(7).

3.2. Harmonics compensation

The controller for harmonics compensation consists of feedforward estimation and feedback control strategy. The feedforward component achieves faster dynamic response with harmonics estimation, while the feedback control loop enhances the system stability as shown in Figure 3 [22]. The feedforward control, as illustrated in Figure 4, is based on current component estimation that is computed on the basis of SVC module current. It is a function of TCR admittance, voltage, and the firing angle α that is updated in each cycle [23]. In a three-phase, three-wire SVC system, three sets of thyristors are triggered at different time. Hence, during steady-state operation of the SVC, three-phase currents have the same waveform with a $\pm 120^o$ shift to each other. However, in case of a change in the firing angle, the three-phase currents lead to change at different time instance. If the feedforward signal is not considered properly, it can cause uncontrollable transients during the reactive power set-point change. The following method has been proposed to overcome this issue.

Since the current of each TCR approaches zero at a 90^o angle to the applied voltage, the trigger angle for next cycle is estimated in a small neighborhood of 90^o and held in sample/hold to calculate the feed-forward

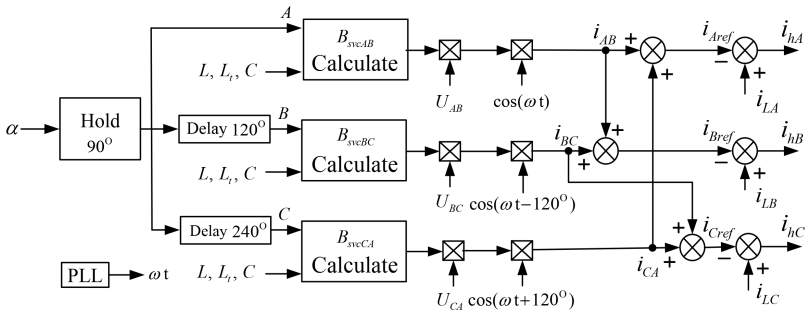

Figure 4. Block diagram of feed-forward control algorithm for APF module.

signal of the next cycle. In Figure 1 TCRs are connected in three-phase delta configuration, while the inductor L and the capacitor C are connected in a three-phase star configuration. For convenience of calculation, the system is transformed to an equivalent form. The reactive current produced by the SVC in the next half cycle can be calculated by:

$$i_{tf_{AB}} = B_{SVC_{AB}} \cdot U \cdot \cos(\omega t), \tag{8}$$

$$i_{tf_{BC}} = B_{SVC_{BC}} \cdot U \cdot \cos(\omega t - 120^o), \tag{9}$$

$$i_{tf_{CA}} = B_{SVC_{CA}} \cdot U \cdot \cos(\omega t + 120^o), \tag{10}$$

where U is the peak value of the line voltage. The SVC branch admittance can be estimated as

$$B_{SVC_j} = \frac{3g(\alpha_i) - \omega^2 L_t C}{3\omega L_t + 9g(\alpha_i)\omega L - 3\omega^3 L_t L C}. \tag{11}$$

The predicted fundamental reactive current of inductor L can be estimated by the following relation:

$$\begin{cases} i^*_{LA} &= i_{tf_{AB}} - i_{tf_{CA}} \\ i^*_{LB} &= i_{tf_{BC}} - i_{tf_{AB}} \\ i^*_{LC} &= i_{tf_{CA}} - i_{tf_{BC}} \\ i^*_{hj} &= i_{Lj} - i^*_{Lj} \end{cases} \tag{12}$$

To estimate the SVC harmonic currents, the total SVC currents i_{Lj} $(j \in \{AB, BC, CA\})$ and the estimated fundamental currents are subtracted from each other. However, the estimated harmonic currents still contain some fundamental current components due to inaccuracies and uncertainties in the system parameters. Thus, these signals are passed through a band reject filter as shown in Figure 3.

The key to designing the feedback controller is the design of the transfer function G_s in Figure 3. It can be seen that G_s consists of two parts. The first part is used to extract fundamental frequency component from the harmonic currents I^*_{hi} and the second part consists of a fundamental frequency band reject filter and a constant gain element K_1. The fundamental frequency component is subtracted from the current I^*_{hi} to extract harmonics component [23] as shown in Figure 4. This process can be expressed as:

$$i_{hi} = i^*_{hi} - i^*_{hif} = (1 - g_1(s))i^*_{hi}, \tag{13}$$

where $g_1(s)$ is the transfer function for fundamental component extraction block. For better accuracy this filter can be synthesized in synchronous reference frame (SRF) as shown in Figure 5. Unlike stationary frame, this method is less sensitive to frequency variation. The following is the expression for this transfer function:

$$g_1(s) = \frac{\frac{s}{T_n} + \omega_o}{\frac{1}{\omega_n \cdot T_n} s^2 + \frac{k_n}{T_n} s + \omega_n^2}, \tag{14}$$

where k_n and T_n are the feedback gain for the nth time and the time constant of the LPF, respectively. The selection of the LPF cutoff frequency is usually $10\% - 20\%$ less than the peak frequency. k_n is the tradeoff between the harmonic rejection capability and the closed-loop stability. Figure 6 shows the bode plot for the transfer function $g_n(s)$ with $n = 1$ and $k_1 = 2.75$.

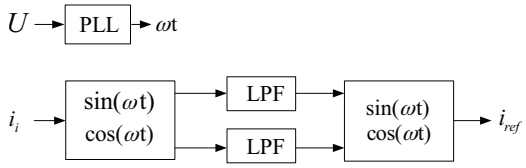

Figure 5. Block diagram of fundamental frequency component extraction method for grid current feed-back control loop based on SRF detection method.

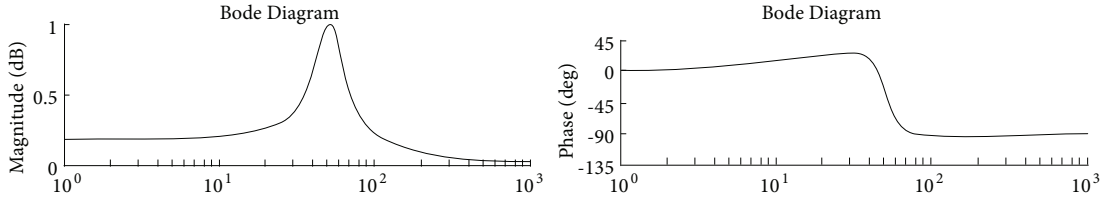

Figure 6. Bode plot for the transfer function $g_n(s)$ with $n = 1$ and $k_1 = 2.75$.

3.3. DC-link voltage control

DC-link voltage has a great influence on the performance of the APF. Therefore, if the DC-link voltage has a larger transition, the APF compensation will either be excessive or insufficient. A small real-power exchange is required between inverter and grid to maintain the DC-link voltages and compensate the inverter losses during a transient state [23].

The control strategy of DC-link voltage for the proposed system is shown in Figure 3. The DC-link voltage error is regulated through the proportional and integral (PI) controller. Further, the output of the PI controller is multiplied by cosine function for phase synchronization with the capacitors current.

$$\mathrm{PI} = 1.5 + \frac{0.2}{s}, \tag{15}$$

$$\begin{cases} v_{dA}^* & = \mathrm{PI} \cdot (U_{ref} - U_{\mathrm{DC}}) \cdot \cos(\omega t), \\ v_{dB}^* & = \mathrm{PI} \cdot (U_{ref} - U_{\mathrm{DC}}) \cdot \cos(\omega t - 120^o), \\ v_{dC}^* & = \mathrm{PI} \cdot (U_{ref} - U_{\mathrm{DC}}) \cdot \cos(\omega t + 120^o). \end{cases} \tag{16}$$

Finally, the active current signal v_d^* is added to the PWM control signal to achieve the DC-link control through real power exchange from the grid.

4. Results and discussion

4.1. Simulated results

To show the performance and effectiveness of the proposed topology and the control scheme, simulation results are obtained using MATLAB/SIMULINK. A three-phase simulation model of 2000 V_{rms} (phase-to-phase) is designed to compensate reactive power in a coal mine with power requirement of each phase between 2 MVAr and 3.2 MVAr.

The selection of the proper capacitor and inductor parameters of the TCR system is based on the voltage and power ratings. The value of filtering inductor L_i depends considerably on the DC-capacitor voltage and on operating frequency. A small value of L_i can improve the power rating fractionally; however, this may lead to poor filtering of harmonics. Similarly, a larger value of L_i leads to better filtering, but its compensation capacity is poor.

Optimal DC-link value should be selected to maintain the DC-capacitors voltages during the transient states and to compensate the inverter losses. In the simulation model, the DC-link capacitor nominal reference voltage has been determined to be 500 V_{DC}. Furthermore, resonant pole of L_i and C_i should not be placed at harmonics frequency. The fundamental frequency reactive current of each phase can be given by the following equation:

$$I_{FL} = \frac{Q_{req}}{V}, \tag{17}$$

$$I_{FL} = \frac{3g(\alpha_i) - \omega^2 L_t C}{3\omega L_t + 9g(\alpha_i)\omega L - 3\omega^3 L_t LC} \times V. \tag{18}$$

The estimated values for L_i and C_i can be obtained by substituting $g(\alpha) = (1, 0)$ for I_{FL} equal to 980 A and 1600 A, respectively. The selection parameters of the system are given in Table 1.

Table 1. Proposed converter components parameters ($i = A$, B, C).

Parameters	Values
L_i	400 µH
L_{ti}	2500 µH
C_i	700 µF
C_{DC}	2800 µF

Figure 7 shows the bode plots for the proposed system presented in Figure 1. The respective parameter values are shown in Table 1. It can be seen that the transfer function magnitude from disturbance to source-side is less than zero beyond 200 Hz. Therefore, the control bandwidth of the proposed system is minimal and the controller is only needed to compensate low-frequency harmonics. Furthermore, a three-phase, three-wire system does not have third harmonics, although it has high levels of fifth and seventh harmonics. Thus, the main purpose of the harmonics compensation control loop, in this case, is to eliminate the fifth and seventh harmonics generated by the TCR.

To design the controller, the parameters are selected based on the control structure described in Section 3. As mentioned earlier, the feed-forward component makes the system faster, while the feedback component plays its part in system stability. The PWM input signals are control output of the system and TCR is the disturbance source. Hence, by using the design guidelines mentioned in Section 3, the control system parameters are obtained as:

$$g_1(s) = \frac{s + 50}{0.024s^2 + 2.75s + 2525}, \tag{19}$$

$$g_5(s) = \frac{4.75s + 57.66}{0.0252s^2 + 4.75s + 62500}, \tag{20}$$

$$g_7(s) = \frac{5s + 69.05}{0.0252s^2 + 5s + 122500}, \tag{21}$$

$k_1 = 2$, $k_5 = 6$, and $k_7 = 4$.

Figure 7a shows the comparison of bode responses with and without feedback APF control. It shall be noted that the magnitude of control input to line current at 50 Hz is less than zero, whereas it is greater than zero within the frequency range 6.3 Hz to 920 Hz. Figure 7b gives the close loop magnitude response bode plot from disturbance to line side with and without controller. It is obvious that the APF can compensate low-order harmonics well and make the system nearly harmonics free. The THD with respect to firing angle is tabulated in Table 2.

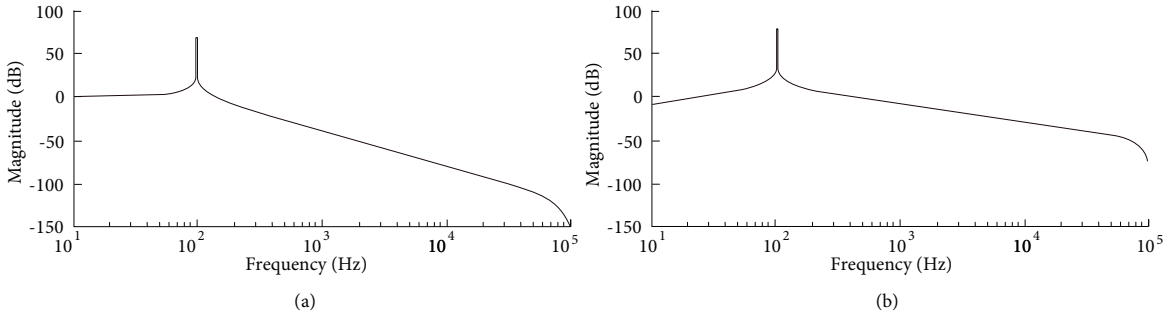

Figure 7. Proposed svc control bode plots: (a) disturbance input to output transfer function bode plot, and (b) control input to output transfer function bode plot

Figure 8 presents steady-state simulation results when the firing angle α is equal to 100°. Figure 8a shows the control input signal of the VSI in terms of VSI output voltages. Figure 8b shows the TCR line current after compensation and in comparison with TCR line current. It can be seen clearly that during the steady state, the voltage variation of the inverter is a small fraction of its DC-link voltages. Figure 8c shows three-phase SVC output current after compensation. It is noted that the output current contains very low harmonics that can be neglected.

The simulated results in Figure 9 show a transient state, where the firing angle changed from 100° to 140° and then back to 100°. It should be noted that the proposed system has fast dynamic response even for a large departure. Figure 9a reveals that the SVC voltage is small and mostly contains fifth and higher order harmonics. It can be seen in Figure 9b that just after the firing angle changes, the amplitude of the control signal has a small transient, implying that the inverter does not need to produce high voltage variations. Figure

Table 2. Simulation results for TCR-module THD (10 cycles).

Firing angle (α^{o})	THD %
90	0.46
100	0.88
110	3.92
120	1.47
130	0.85
140	0.47
150	0.27
160	0.16
180	0.09

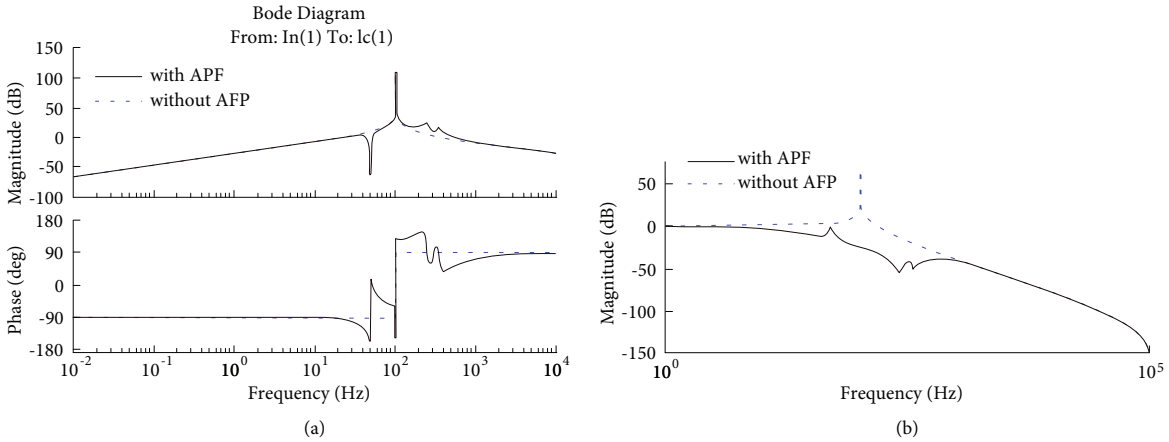

Figure 8. Bode plot to show the effectiveness of system with and without control. (a) Magnitude and phase plot for control input to line side current with and without controller and (b) close loop magnitude response bode plot from disturbance to line side with and without controller.

9c clearly shows that the transitions in firing angle have a small influence on the SVC output current, and the response time of the system is less than half a cycle. For the given system parameters, the system works well with a 500 V DC-link reference. Hence, for a three-phase system, the SVC voltage rating is 25% of the line voltage to fulfill the requirements for the whole operating range.

Figure 10 shows the DC-link capacitor voltages under steady-state operation and firing angle change. Figure 10a shows that the voltage of the DC-link capacitor has less than 1% ripple with respect to the DC-link voltage reference. Figure 10b shows the transient response of the DC-link voltage when firing angle is changed on the basis of Figure 9. It is obvious that the DC-link controller performs well in the proposed topology. Table 2 gives the values for total harmonic distortion (THD) of the SVC system at different firing angles.

4.2. Experimental results

To verify the aforementioned analysis and simulated results, a three-phase TCR downscaled prototype was constructed and evaluated. The passive component parameters were the same as those used in the simulation model. However, the voltage of the system was set to 380 V, and 110 V was chosen for (U_{DC}) DC-link. The system parameters are listed in Table 3.

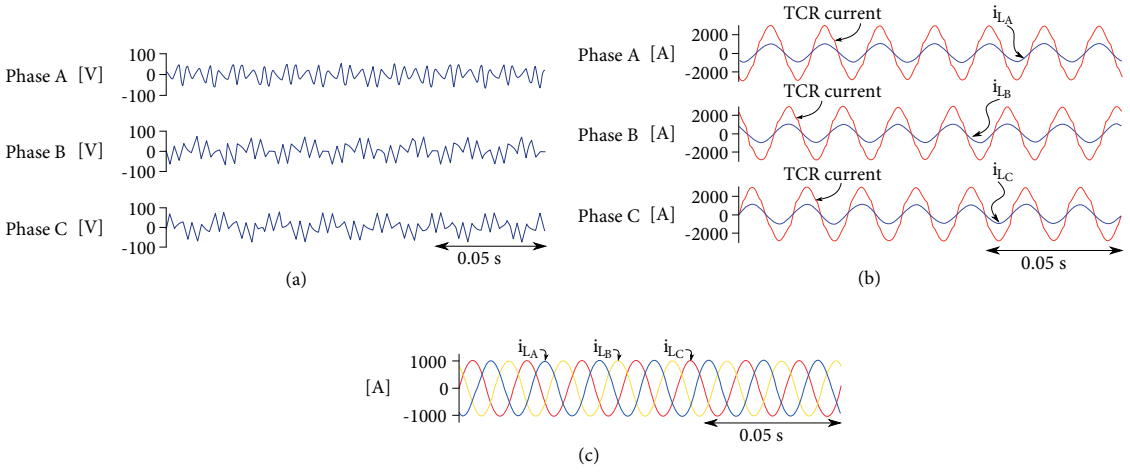

Figure 9. Simulated waveform to response of the TCR-module system for firing angle $\alpha = 100^{o}$. (a) Control signals, (b) TCR current after compensation, and (c) three-phase SVC output currents.

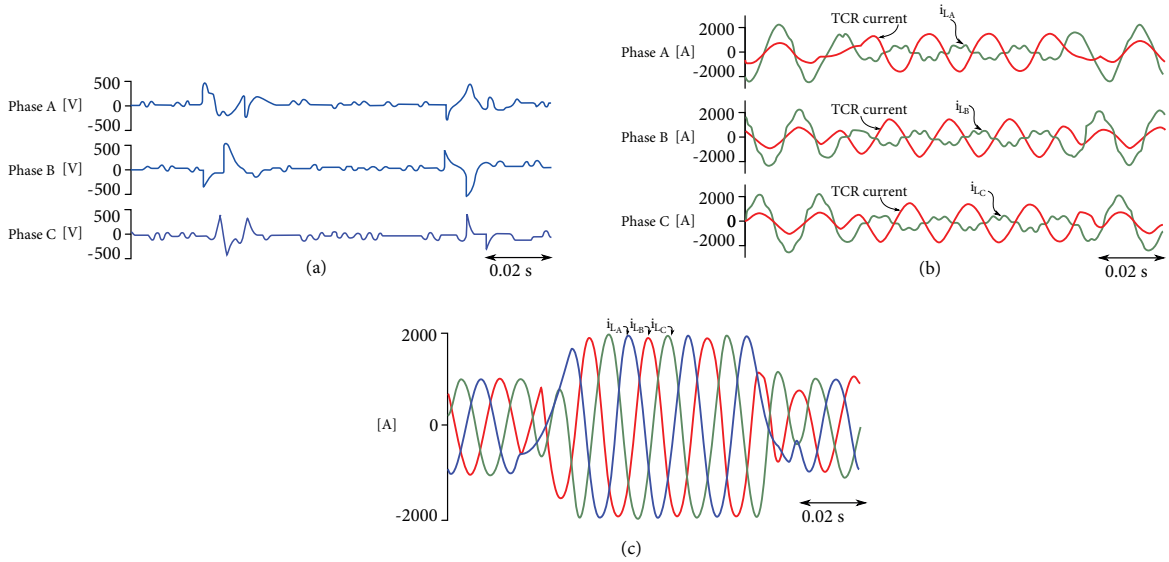

Figure 10. Simulated waveform to show the effectiveness of proposed control in a transient state for step change in firing angle, from $100^{o} - 140^{o} - 100^{o}$. (a) Control signals, (b) TCR currents per phase and SVC output currents, and (c) three-phase SVC currents after compensation.

A three-phase inverter was used to serve as an APF. The three-phase VSI is controlled by using a 6.4 kHz PWM signal generated by Texas Instrument digital signal processor TMS320F28335. The DSP is responsible for the soft startup, software PLL, APF current control, DC-link control, and TCR firing angle control. The single line block diagram of the proposed SVC laboratory prototype is shown in Figure 11. Two kinds of simulated and experimental tests were conducted. Initially the system was run and tested under steady-state operation then the transient effect of the system was checked.

The simulated and experimental waveforms under steady-state operation are shown in Figure 12a. Due to four channels scope, only single-phase inductor I_{L_A}, capacitor I_{C_A}, and TCR I_{TCR_A} currents are shown in Figure 12a. The firing angle was set to 140^{o} in simulation and experimental setup. The three-phase steady-

Table 3. Experimental component parameters ($i = A, B, C$).

Parameters	Values
Switching frequency	6.4 kHz
Grid voltage (U_{AC})	380 V
DC-link voltage (U_{DC})	110 V
DSP control board	TMS320F28335
L_i	400 µH
L_{ti}	2500 µH
C_i	700 µF
C_{DC}	2800 µF

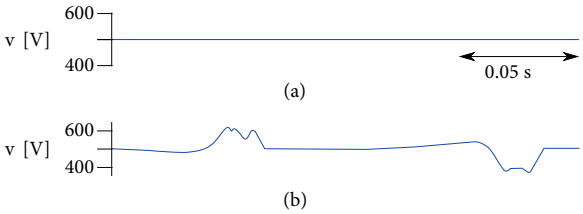

Figure 11. Simulated waveform of DC-link voltage under steady state and transient state: (a) stable situation and (b) firing angle change.

state simulated and experimental test results of inductor currents are shown in Figure 12b. The presented experimental results show good consistency with the simulated waveforms.

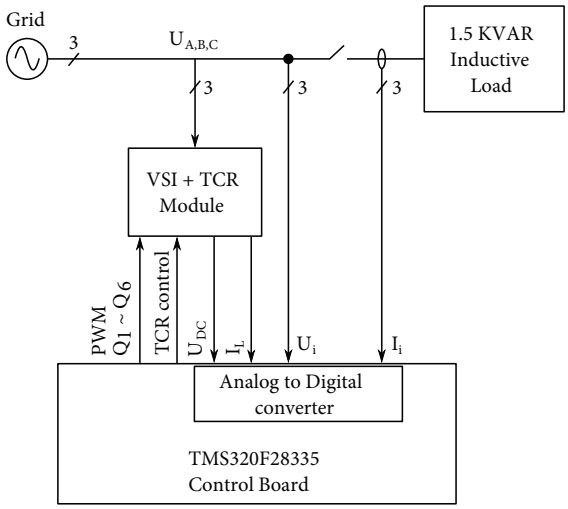

Figure 12. Single line block diagram of the proposed SVC laboratory prototype.

The dynamic performance of the system is also tested. Figure 12c shows the simulated and experimental waveforms in a transient state with sharp change. Note that during transient state the inductor, capacitor, and TCR currents converge to reference in short time. The three-phase inductor current simulated and experimental

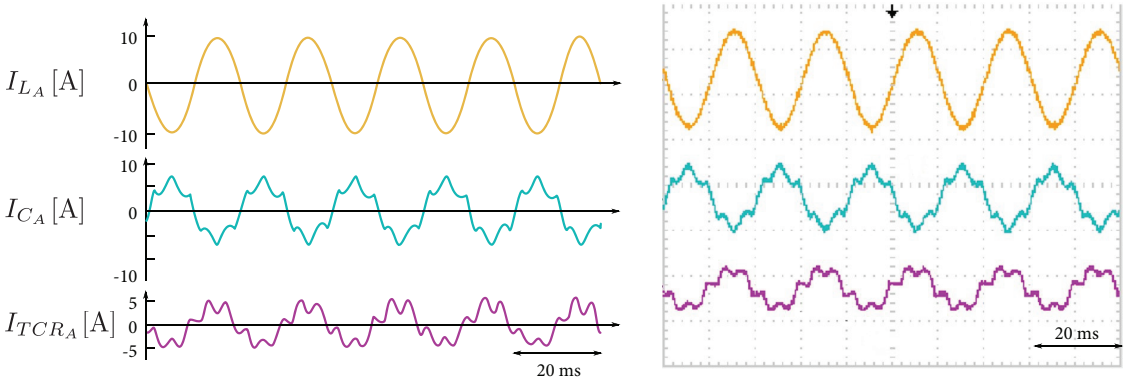

Figure 13. Simulated and experimental waveforms of Phase A steady-state response for firing angle of 140°. The inductor current I_{L_A}, capacitor current I_{C_A}, and TCR current I_{TCR_A} (yaxis: 10 A/div).

waveforms are shown in Figures 12d. However, the experimental transient responses shown in Figure 12c and 12d are a little slower as compared to the responses from the simulation. This is due to the construction limitation of the real prototype, but the same trend can be seen. Table 4 shows that after enabling the APF control system, three-phase current THD values are significantly reduced. The proposed APF shows good performance of harmonic suppression.

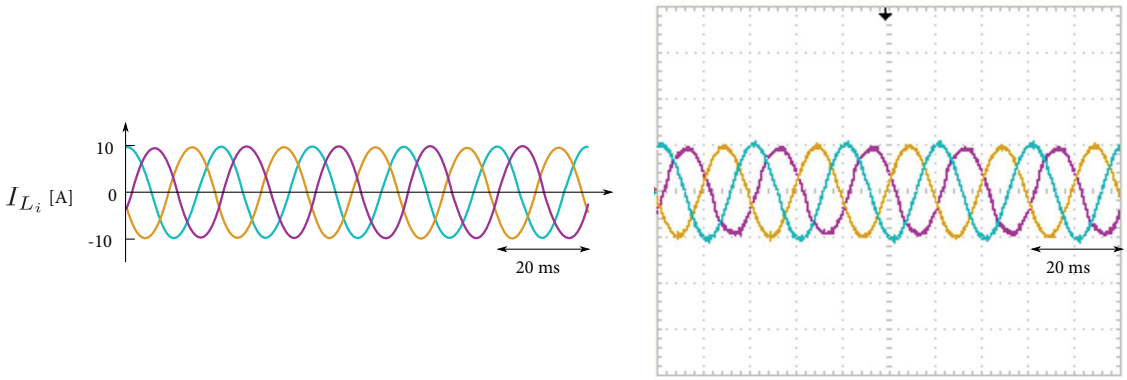

Figure 14. Simulated and experimental waveforms of Phase A, B, and C steady-state response for firing angle of 140°. The inductor current I_{L_i} (yaxis: 10 A/div).

5. Conclusion

This paper proposes a new topology of hybrid active power filter for a three-phase SVC power system. An alternative filter design has been proposed and applied to the TCR to minimize the harmonics distortion in the system. To meet the requirements of this new filter, a new control scheme is proposed and analyzed. A system design example at low medium voltage level has shown the efficacy of the proposed system. Simulated and experimental results have shown that the new topology of SVC can perform better than the traditional harmonic mitigation methods used in the past. Based on proposed feedback and feedforward control, the system stability and response time have improved.

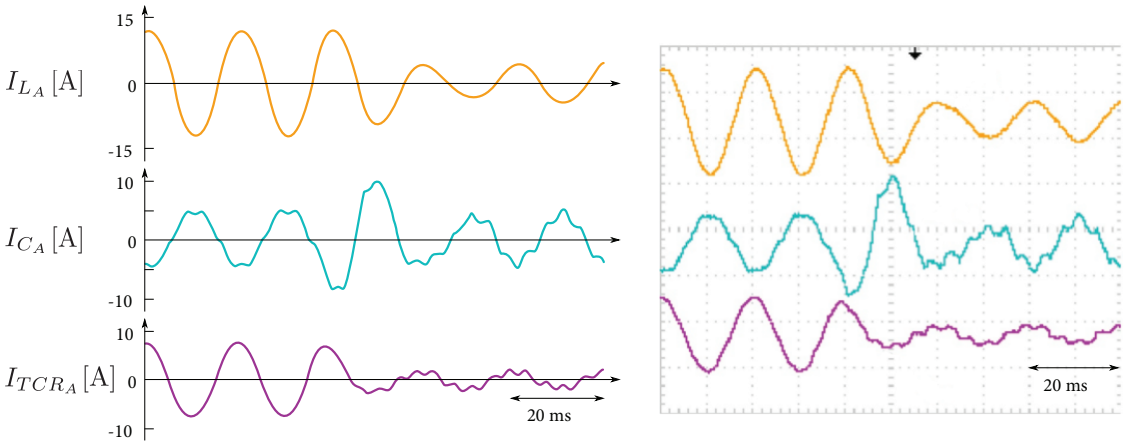

Figure 15. Simulated and experimental waveforms of Phase A steady-state response for firing angle of 140°. The inductor current I_{L_A}, capacitor current I_{C_A}, and TCR current I_{TCR_A} (yaxis: 10 A/div).

Table 4. THD (10 cycles) analysis of experimental results for TCR-module.

Firing angle (α^o)	With APF	Without APF
	THD %	THD %
90	1.56	4.35
100	2.12	6.25
110	2.92	8.02
120	3.22	9.34
130	4.37	12.58
140	5.10	13.16
150	3.27	10.87
160	2.60	5.10
180	1.42	4.40

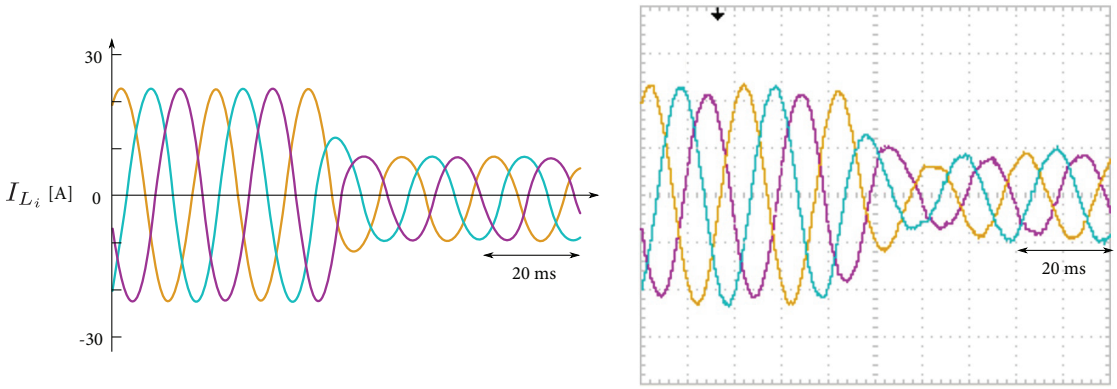

Figure 16. Simulated and experimental waveforms of Phase A, B, and C transient state response for firing angle 100° − 140°. The inductor current I_{L_i} (yaxis: 20 A/div).

Acknowledgment

The authors would like to thank Khan MM from Changzhou Tianman Energy Technology, for the fruitful discussions and support with this topic.

Author Contributions

Humayun M and Ul Hassan M proposed the idea, suggested the literature and supervised in writing the manuscript. Y. Xuhui and W. Feng helped in system parameters and designing to make the simulation and practical test possible and shared the summary of various credible articles to be included in this manuscript.

References

[1] Padmavathi SV, Sahu SK, Jayalaxmi A. Modeling and simulation of static VAR compensator to enhance the power system security. In: 2013 IEEE Asia Pacific Conference on Postgraduate Research in Microelectronics and Electronics (PrimeAsia); Visakhapatnam, India; 2013. pp. 52-55. doi: 10.1109/PrimeAsia.2013.6731177c

[2] Chang GW, Liu YJ, Dinavahi V, Su HJ. On real-time simulation for harmonic and flicker assessment of an industrial system with bulk nonlinear loads. IEEE Transactions on Industrial Electronics 2010; 57 (9): 2998-3009. doi: 10.1109/TIE.2009.2037645

[3] Kefalas TD, Kladas AG. Harmonic impact on distribution transformer no-load loss. IEEE Transactions on Industrial Electronics 2010; 57 (1): 193-200. doi: 10.1109/ICIAS.2007.4658507

[4] Enslin JH, Heskes PJ. Harmonic interaction between a large number of distributed power inverters and the distribution network. IEEE Transactions on Power Electronics 2004; 19 (6): 1586-1593. doi: 10.1109/TPEL.2004.836615

[5] Daratha N, Das B, Sharma J. Coordination between oltc and SVC for voltage regulation in unbalanced distribution system distributed generation. IEEE Transactions on Power Systems 2014; 29 (1): 289-299. doi: 10.1109/TPWRS.2013.2280022

[6] Tey L, So P, Chu Y. Improvement of power quality using adaptive shunt active filter. IEEE Transactions on Power Delivery 2005; 20 (2): 1558-1568. doi: 10.1109/TPWRD.2004.838641

[7] Kkedra B. Reducing inverter power rating in active power filters using proposed hybrid power filter topology. In: 2015 IEEE 15th International Conference on Environment and Electrical Engineering (EEEIC); Rome, Italy; 2015. pp. 443-448. doi: 10.1109/EEEIC.2015.7165203

[8] Ginarsa IM, Soeprijanto A, Purnomo MH, Hiyama T. Controlling voltage collapse using anfis-based composite controller-SVC in power systems. In: 2011 IEEE Region 10 TENCON Conference; Bali, Indonesia; 2011. pp. 74-78. doi: 10.1109/TENCON.2011.6129066

[9] Mandal S, Kolluri VS. Coordinated capacitor bank switching using SVC controls. 21st IEEE Century in the Power and Energy Society General Meeting-Conversion and Delivery of Electrical Energy; Pittsburgh, PA, USA; 2008. pp. 1-7. doi: 10.1109/PES.2008.4596539

[10] Biricik S, Komurcugil H. Three-level hysteresis current control strategy for three-phase four-switch shunt active filters. IET Power Electronics 2016; 9 (8): 1732-1740. doi: 10.1049/iet-pel.2015.0764

[11] Rahmani S, Mendalek N, Al-Haddad K. Experimental design of a nonlinear control technique for three-phase shunt active power filter. IEEE Transactions on Industrial Electronics 2010; 57(10): 3364-3375. doi: 10.1109/TIE.2009.2038945

[12] Wang L, Lam CS, Wong MC. Minimizing inverter capacity design and comparative performance evaluation of SVC-coupling hybrid active power filters. IEEE Transactions on Power Electronics 2018; 34 (2): 1227-1242. doi: 10.1109/TPEL.2018.2828159

[13] Singh A, Baredar P. Power quality analysis of shunt active power filter based on renewable energy source. In: 2014 IEEE International Conference on Advances in Engineering and Technology Research (ICAETR); Unnao, India; 2014. pp. 1-5. doi: 10.1109/ICAETR.2014.7012836

[14] Luo A, Shuai Z, Zhu W, Shen ZJ. Combined system for harmonic suppression and reactive power compensation. IEEE Transactions on Industrial Electronics 2009; 56 (2): 418-428. doi: 10.1109/TIE.2008.2008357

[15] Junling C, Yaohua L, Ping W, Congzhe G, Xinjian J et al. A novel control method for a combined system using active power filter and static VAR compensator. In: 2010 IEEE International Conference on Electrical Machines and Systems (ICEMS); Incheon, South Korea; 2010. pp. 334-337.

[16] Dong T, Li L, Ma Z. A combined system of apf and SVC for power quality improvement in microgrid. In: 2012 IEEE Power Engineering and Automation Conference (PEAM) 2012; Wuhan, China; 2012. pp. 1-4. doi: 10.1109/PEAM.2012.6612554

[17] Junling C, Yaohua L, Ping W, Zhizhu Y, Zuyi D. A novel combined system using cascaded active power filter and static VAR compensator for high-power applications. IEEE International Conference on Computer Distributed Control and Intelligent Environmental Monitoring (CDCIEM); Changsha, China; 2011. pp. 664-667. doi: 10.1109/CDCIEM.2011.131

[18] Khan MM, Rana A. Thyristor-controlled susceptance design based on reduced power switching compensator. IET Power Electronics 2014; 7 (12): 3159-3168. doi: 10.1049/iet-pel.2013.0647

[19] Köse, Ali, Irmak E. Modeling and simulation of a static VAR compensator based on FC-TCR. In: 2016 IEEE International Conference on Renewable Energy Research and Applications (ICRERA); Birmingham, UK; 2016. pp. 924–927. doi: 10.1109/ICRERA.2016.7884470

[20] Czarnecki L, Hsu S. Thyristor controlled susceptances for balancing compensators operated under nonsinusoidal conditions. IEEE Proceedings Electric Power Applications 1994; 141 (4): 177-185. doi: 10.1049/ip-epa:19949984

[21] Mokhtari M, Golshannavaz S, Nazarpour D, Farsadi M. Control of an SVC for the load balancing and power factor correction with a new algorithm based on the power analysis. IEEE Power Quality Conference (PQC); Tehran, Iran; 2010. pp. 1-5.

[22] Castro LM, Acha E. A unified modeling approach of multi-terminal VSC-HVDC links for dynamic simulations of large-scale power systems. IEEE Transactions on Power Systems 2016; 31 (6): 5051-5060. doi: 10.1109/TPWRS.2016.2527498

[23] Han Y, Xu L, Khan MM, Chen C, Yao G et al. Robust deadbeat control scheme for a hybrid apf with resetting filter and adaline-based harmonic estimation algorithm. IEEE Transactions on Industrial Electronics 2011; 58 (9): 3893-3904. doi: 10.1109/TIE.2010.2093475